Flotation separation of pyrite and chalcopyrite with potassium permanganate as a depressant

Qinbo Cao (qinbocao@kust.edu.cn)
Kunming University of Science and Technology https://orcid.org/0000-0002-8175-7595
Haiyu Zhang
Kunming University of Science and Technology
Yan Yan
Kunming University of Science and Technology
Yanjun Li
Kunming University of Science and Technology
Dianwen Liu
Kunming University of Science and Technology

Research Article

Keywords: potassium permanganate, depressant, chalcopyrite, pyrite

Posted Date: August 17th, 2023

DOI: https://doi.org/10.21203/rs.3.rs-3221139/v1

Version of Record: A version of this preprint was published at Chemical Papers on December 4th, 2023.
See the published version at https://doi.org/10.1007/s11696-023-03203-6.

Abstract

This paper used potassium permanganate ($KMnO_4$) as a pyrite depressant to separate pyrite from chalcopyrite. Flotation and contact angle results indicated that pyrite could be depressed by $KMnO_4$ at pH 7, while $KMnO_4$ treated chalcopyrite could be floated by sodium ethylxanthate. Zeta potential analysis revealed that $KMnO_4$ oxidized the pyrite surface, lowering its hydrophobicity. The oxidation products on the pyrite surface were FeO, FeOOH and $Fe_2(SO_4)_3$ as determined by XPS analyses. These oxidation products were well coated on the pyrite surface, which dramatically lowers the hydrophobicity of pyrite. In contrast, in the case of chalcopyrite, $KMnO_4$ treatment did not generate new oxidation components on its surface, causing chalcopyrite surface to remain hydrophobic and allowing the flotation of chalcopyrite by air bubbles. Thus, pyrite could be efficiently separated from chalcopyrite using $KMnO_4$ as a depressant.

Introduction

Copper is a crucial strategic metal for most countries (Ding et al., 2022), widely used in metallurgy, daily necessities, industry, defense industry, and other fields (Wu et al., 2022). Chalcopyrite ($CuFeS_2$) is the primary source of copper metal (Wu et al., 2022) and coexists with other sulfide minerals in the natural ore deposits, especially pyrite (FeS_2) (Zhang et al., 2023). Froth flotation is the primary method of enriching chalcopyrite. However, because the natural floatability of pyrite is better than chalcopyrite (Moimane et al., 2021), pyrite can be readily enriched in the chalcopyrite concentrate (Owusu et al., 2014). The pyrite in chalcopyrite concentrate lowers the copper grade but raises the grades of iron and sulfur in the concentrate, which deteriorates the subsequent smelting processes (Khoso et al., 2019). Therefore, the copper concentrates used for smelting should have a copper grade of at least 13%. In this regard, pyrite must be separated from chalcopyrite in the flotation process.

Lime (CaO) is a common pyrite depressant used in the flotation separation of pyrite and chalcopyrite (Liu et al., 2020a). Due to the low price of lime, this depressant has been applied in most beneficiation plants in China (Bai et al., 2021). However, lime has some drawbacks in the flotation system. First, lime shows a poor ability to depress pyrite because of its low solubility in water. In the case of a run-of-mine ore with high content of pyrite, it is difficult to completely prevent pyrite flotation by lime. Second, the presence of lime in pulp results in calcium hydroxide ($Ca(OH)_2$) precipitation. Such precipitation blocks the pipes in plants (Han et al., 2020). Therefore, more efficient depressants are still needed for most flotation plants in China.

Currently, a number of inorganic depressants have been developed for the separation of chalcopyrite and pyrite, such as H_2O_2 (Khoso et al., 2019), $Ca(ClO)_2$ (Wang et al., 2020), Na_2CO_3(Liu et al., 2020b), and Na_2SO_3 (Pan et al., 2022). These depressants could oxidize the pyrite surface, generating hydrophilic species, such as FeO, FeOOH, and $Fe_2(SO_4)_3$. As a result, the pyrite surface becomes hydrophilic, and the pyrite flotation can be prevented(Wei et al., 2019). On the other hand, the development of organic depressants is attracting considerable attention, as organic depressants show limited environmental

impact compared to inorganic reagents. The organic depressants used for pyrite flotation include dextrin (Dong et al., 2021), biopolymers (Mu et al., 2018), starch (Han et al., 2019), guar gum (Chen et al., 2018), CMC (Wang et al., 2022), and lignosulfonates (Chen et al., 2021). These organic depressants typically have multiple hydroxyls groups and can adsorb on the pyrite surface, producing a hydrophilic surface. However, organic depressants are very sensitive to gangue minerals, such as quartz, and their prices are higher than inorganic reagents. Thus, flotation plants tend to use efficient inorganic reagents.

Potassium permanganate ($KMnO_4$) is a high-efficiency depressant and powerful oxide for many minerals. Therefore, the depressing ability of $KMnO_4$ has received much attention in the past decade. $KMnO_4$ could amplify the recovery gap between galena and sphalerite (Chen et al., 2022). It is reasonable to expect that $KMnO_4$ could be used as a depressant for pyrite flotation. However, the adsorption features of $KMnO_4$ in pyrite-chalcopyrite flotation systems are still not fully understood. Therefore, it is necessary to investigate the role of $KMnO_4$ in the pyrite and chalcopyrite system.

In this regard, the aim of this paper was to assess the depressing capacity of $KMnO_4$ in the pyrite and chalcopyrite system. Flotation and contact angel methods were employed to investigate the depressing features of $KMnO_4$ on pyrite and chalcopyrite flotation. The oxidization species on the pyrite and chalcopyrite surfaces were identified by XPS analysis. Moreover, SEM experiments were conducted to investigate the distribution of oxidization products on the pyrite surface.

Experimental and calculation details

Materials and reagents

Pyrite and chalcopyrite samples were taken from Yunnan Province, China. XRF analysis indicated that the grades of Fe and S in pyrite samples were 44% and 50.12% respectively, and the grades of Cu, Fe and S in chalcopyrite samples were 34.17%, 29.30% and 30.92% respectively (Table 1). Thus, the results of XRF analysis confirmed the high purity of pyrite and chalcopyrite samples. While XRD analysis indicated that only pyrite and chalcopyrite were found in the samples (Fig. 1), which was confirmed the high purity of the sample. $KMnO_4$ and sodium ethylxanthate (SEX) were both analytical reagents (AR)-grade from Sinopharm Chemical Reagent Co., Ltd., China. Terpineol was from Zhuzhou Sanlin Chemicals Ltd., China. Ltd. Hydrochloric acid (HCl) and sodium hydroxide (NaOH) were used to adjust the pH of the solutions (Kelon Chemical Reagent Factory, Chengdu, China). All experiments were conducted with deionized (DI) water with a resistivity of 18.25 MΩ•cm at 23°C. The minerals were ground 38 − 74 μm particles for the flotation experiments and SEM experiments. Pure pyrite or chalcopyrite with a particle size of −5 μm was used for surface examinations.

Table 1
XRF results of pure mineral samples (wt. %).

Mineral	Cu	Fe	S	Zn	Ca	Al	Si	As	Sb
Pyrite	-	44.00	50.12	0.05	0.70	0.07	0.67	0.11	-
Chalcopyrite	34.17	29.30	30.92	0.59	-	0.09	0.09	-	0.09

Flotation tests

The XFG II flotation machine and a 40-mL flotation cell (Jilin Province Ore Exploration Machinery Factory, Changchun, China) were used in Single-mineral flotation tests. 2 g of mineral (38 − 74 μm) was added into $KMnO_4$ solution. During the treatment, the stirring speed was 400 r/min. After the oxidization, the suspension was transferred into the flotation cell. SEX and terpineol were sequentially added to the suspension and conditioned for 3 min and 1 min, respectively. The mineral was floated for 2 min. The froth and sink products were weighed and calculated recovery separately. The impeller speed of the flotation machines was 1600 rpm and the airflow rates were 1.16 L/min. For mixed minerals experiments, pyrite (1.0 g) and chalcopyrite (1.0 g) were placed into $KMnO_4$ solution. The sample preparation for mixed mineral flotation were the same as those for single mineral flotation. The experiments were repeated three times and the average recovery was reported.

Contact angle measurements

The contact angle measurements were carried out with JY-82 instrument (China). Before the measurements, the crystal minerals were cut into 20 mm ×15 mm pieces. The surface of each sample was rinsed with ethanol and DI water to remove organics and then dried in air. Further, the sample surface was polished with 2000 and 6000 grit sandpapers to obtain a smooth surface. The polished surface was rinsed with DI water and dried under vacuum. The three-phase contact line on the surface was formed by dropping an approximately 2 mm DI water droplet on the sample surface. Then the contact angle was determined. The measurement was repeated three times and the errors of measurements were less than ± 2°. The reported results are the mean values of the three measurements.

Electrokinetic analyses

Zeta potential measurements were conducted using a ZETASIZER Nano-Zs90 series instrument (Malvern Instruments, UK). All of the measurements were performed with 1×10−3 mol/L KCl as the background electrolyte solution. The mineral suspension was prepared by dispersing 0.02 g of the mineral into 40 mL of the KCl solution. Each suspension was stirred for 4 min (300 r/min) with/without SEX and $KMnO_4$. The suspension was allowed to settle for 5 min, and the supernatant containing the finer particles was transferred to a capillary cell to determine the electrophoretic mobility. Each sample was measured by three times.

X-ray photoelectron spectroscopy (XPS) analysis

The XPS study was conducted by a PHI5000 Versaprobe II equipped with an Al Kα source. The XPS spectra were further fitted with MultiPak Spectrum software. All spectra were calibrated based on the C1s spectra with a binding energy of 284.8 eV. The XPS samples were prepared in the same manner as those for the electrokinetic analysis.

SEM-EDS experiments

A JEOL JSM-6360 instrument was employed to measure the elemental composition of the pyrite and chalcopyrite surfaces, which were examined at an accelerating voltage of 20.0 kV. Both the natural and oxidized samples were examined for comparison. In terms of the oxidized samples, pyrite or chalcopyrite (2.0 g, 38 − 74 μm) was placed in 100 ml $KMnO_4$ solution and stirred for 4 min. After the KMnO4 treatment, the samples were filtered and dried in a vacuum tank.

Results and discussion

Effect of pH on the flotation behavior

Previous studies have demonstrated that the slurry pH is a vital factor for pyrite and chalcopyrite flotation (Zhang et al., 2023). Here, the influence of pH on the depressing capacities of $KMnO_4$ (3 min of treatment) for pyrite and chalcopyrite were determined by flotation tests in the pH region of 3–11. In addition, the concentration of SEX was 5×10^{-4} mol/L in the flotation tests.

For natural pyrite, the maximum recovery (90%) was achieved at pH 7 (Fig. 2a). Acidic and alkaline solution were not beneficial to pyrite flotation. For example, the pyrite recoveries were only 75% and 76% at pH 3 and 11. A similar trend was also found in previous work (Khoso et al., 2019). The pyrite surface may be adsorbed by hydroxide ions in an alkaline solution, reducing the hydrophobicity of pyrite and lowering the pyrite recovery (Niu et al., 2019; Wang et al., 2021; Zhang et al., 2023). On the other hand, the SEX collector may be unstable in an acidic solution (Niu et al., 2019; Wang et al., 2021), resulting in a unsatisfactory recovery.

When pyrite was treated with 1×10^{-4} mol/L of $KMnO_4$, the pyrite recoveries were in the region of 40–50% at each examined pH (Fig. 2b), indicating that SEX could not float these samples. Furthermore, the recovery gap between $KMnO_4$-treated and natural pyrite samples reached 50% at pH 7, which is the highest gap observed under all tested pH values. It appears that pH 7 is the optimal condition for $KMnO_4$ to depress pyrite flotation.

The flotation behavior of chalcopyrite was also examined for comparison. The chalcopyrite recoveries ranged from 80–90% in the pH region of 3–11 (Fig. 2b). it seems that the pH of solution had little effect on the flotation of chalcopyrite with SEX, which is in line with the previous report (Khoso et al., 2019). In terms of the $KMnO_4$-treated chalcopyrite, the recovery was slightly lowered by 3–5% compared to that of natural chalcopyrite at the same pH. These results suggested that $KMnO_4$ was not an efficient

chalcopyrite depressant. In this regard, $KMnO_4$ could be used as a specific depressant for pyrite rather than chalcopyrite. On the other hand, the pyrite recovery reached 71% with 5.65×10^{-3} mol/L of lime, which is 30% higher than that by 1×10^{-4} mol/L of $KMnO_4$ at same oxidization time (Fig. S1). This finding suggests that $KMnO_4$ is a more efficient depressant for pyrite.

Effects of KMnO4 concentration and oxidation time

The above flotation results illustrated that pH 7 is appropriate for the separation of pyrite from chalcopyrite with $KMnO_4$ as a depressant. To further determine the depressing ability of $KMnO_4$, the impact of $KMnO_4$ concentration and oxidation time on the flotation behaviors of pyrite and chalcopyrite were investigated in this part. The pH and SEX concentration in the flotation tests were controlled as pH 7 and 5×10^{-4} mol/L.

The recovery of natural pyrite was 90% (Fig. 3a), suggesting that the natural pyrite has a good floatability (Jiang et al., 2023). When pyrite was treated by 1×10^{-4} mol/L of $KMnO_4$, the recovery of pyrite decreased sharply with the increase in oxidation time. However, when the oxidation time was higher than 3 min, the pyrite recovery reduced to a stable value (nearly 40%). The same trend was observed for the treatment with 3×10^{-4} or 5×10^{-4} mol/L of $KMnO_4$. It seems that 3 min of oxidization is enough for $KMnO_4$ to depress pyrite. Moreover, pyrite recovery with 3×10^{-4} mol/L of $KMnO_4$ (32.14%) was close to that (27.67%) with 5×10^{-4} mol/L of $KMnO_4$ after 3 min of oxidization time. Such results imply that 3×10^{-4} mol/L of $KMnO_4$ is reasonable to inhibit the flotation of pyrite.

In contrast, the chalcopyrite recovery was hardly altered by the treatment with 1×10^{-4} mol/L of $KMnO_4$.. The chalcopyrite recovery was still 95% after 5 min of oxidization with 1×10^{-4} mol/L of $KMnO_4$ (Fig. 3b). Differently, as the $KMnO_4$ concentration increased to 3×10^{-4} or 5×10^{-4} mol/L, the chalcopyrite recovery was reduced by 15% after 3 min of = treatment compared to that of natural chalcopyrite. It appears that high $KMnO_4$ concentration treatment may deteriorate the chalcopyrite flotation to some degree. However, chalcopyrite recovery was still 50% higher than pyrite, when both minerals were reacted with 3×10^{-4} $KMnO_4$ for 3 min. These findings indicate that $KMnO_4$ has a strong depressing capacity for pyrite over chalcopyrite.

Moreover, the flotation tests of pyrite and chalcopyrite mixture were performed to further examine the depression efficiency of $KMnO_4$ (Fig. 4), since single-mineral flotation results are less representative for a real flotation system (Liu and Liu, 2004). The separation efficiency (SE) was calculated using the following equation to analysis the depression selectivity of $KMnO_4$ for the pyrite-chalcopyrite mixture (Bahrami et al., 2018):

$$SE=\frac{Cm(c-f)}{Ff(m-f)}$$

Where C and F are the dried weights of the concentrate and feed, m is the Cu grade in the chalcopyrite sample, c and f are the Cu grades of concentrate and feed.

the SE index results depending on the $KMnO_4$ concentration on could be divided into two distinctive regions. In region I, from 1×10^{-4} to 4×10^{-4} mol/L $KMnO_4$, the Cu recoveries were maintained at nearly 95%, and the SE increased from 33–88%. These results imply that chalcopyrite was well floated by SEX in this $KMnO_4$ concentration region and pyrite could be depressed by $KMnO_4$. Thus, the increases in $KMnO_4$ concentration in this region improve the SE index. However, when the $KMnO_4$ concentration was over 4×10^{-4} mol/L, i.e., region 2, the further increase in $KMnO_4$ concentration lowered the Cu recovery, and the SE was also reduced. It is expected that a higher $KMnO_4$ concentration may result in an oxidization of chalcopyrite surface, producing the hydrophilic SO-2 4 specie that causes a decrease in chalcopyrite recovery during flotation (Khoso et al., 2019). Therefore, 4×10^{-4} mol/L of $KMnO_4$ is suitable for the separation of pyrite from chalcopyrite.

Difference in the hydrophobicity between pyrite and chalcopyrite

The above flotation results showed that $KMnO_4$ could be used as a specific depressant for pyrite. To further clarify the depressing behavior of $KMnO_4$, the change in the hydrophobicity of pyrite and chalcopyrite surfaces was evaluated by contact angle experiments, since the hydrophobicity of pyrite or chalcopyrite surface determines the flotation performance of such sulfide mineral. The pyrite and chalcopyrite crystals were preconditioned with 4×10^{-4} mol/L of $KMnO_4$ at pH 7 for the contact angle study.

For chalcopyrite, the contact angle of the natural surface was measured to be 71.5° (Fig. 5), which was consistent with the previous reports (Deng et al., 2017; Li et al., 2019; Wu et al., 2022). The condition with $KMnO_4$ solution was unable to reduce the contact angle of chalcopyrite surface efficiently. The contact angle was still 64.44° after 5 min of $KMnO_4$ treatment. Our flotation tests also demonstrated that 4×10^{-4} mol/L of $KMnO_4$ condition hardly reduced the floatability of chalcopyrite. Thus, it is elucidated that 4×10^{-4} mol/L of $KMnO_4$ could not oxidize chalcopyrite surface to produce hydrophilic species on the mineral surface.

In the case of pyrite, the contact angle of the natural surface was 62.4°. Similar results were reported in early works (Deng et al., 2017; Li et al., 2019; Wu et al., 2022). Due to its superior hydrophobicity, pyrite can be floated by a collectorless flotation strategy (Ma et al., 2022; Pan et al., 2022). The contact angle of pyrite decrased with the increasing $KMnO_4$ treatment time. Since $KMnO_4$ is a strong oxidizer, it may oxidize the pyrite surface, generating hydrophilic species and lowering the contact angle. It was observed that the contact angle was reduced to a stable value, i.e., 22°, as the $KMnO_4$ condition time exceed 3 min. It is expected that the pyrite surface was well coated by oxidized species after 3 min of $KMnO_4$ treatment, which prevents the pyrite flotation.

In this regard, our flotation and contact angle results both revealed that $KMnO_4$ could oxidize pyrite prior to chalcopyrite. Moreover, the flotation separation of these two minerals could be achieved by carefully controlling the $KMnO_4$ concentration (4×10^{-4} mol/L) and oxidation time (3 min).

Zeta potential analyses

Zeta potential analysis has been widely used to determine the adsorption of charged ions and collectors on mineral surfaces. The zeta potentials of pyrite and chalcopyrite in DI water, SEX and $KMnO_4$ solutions (4×10^{-4} mol/L) were compared in this section, to further understand the depression behavior of $KMnO_4$.

For nature pyrite, the isoelectric point (pH_{iep}) of pyrite was approximately pH 5.5 (Fig. 6a). Similar results were reported in the previous works (Hong et al., 2017; Khoso et al., 2019; Mu et al., 2016). When pyrite was conditioned with SEX solution, the zeta potential of pyrite shifted to a more negative value compared to that of natural pyrite at the same pH. It is expected that xanthate anions could adsorb on the pyrite surface, thereby lowering the zeta potential.

When pyrite was treated by $KMnO_4$ solution, the zeta potential of pyrite shifted towards a more positive value compared to the results of pyrite in DI water. It seems that the $KMnO_4$ treatment induced the formation of oxidized products on the pyrite surface, and such oxidized products raised the zeta potential of pyrite. A similar trend was also found in the previous literature where H_2O_2 was used as a depressor and oxidant for pyrite (Khoso et al., 2019). Moreover, when the $KMnO_4$-treated pyrite was conditioned with SEX, SEX was unable to efficiently reduce the zeta potential of pyrite. For example, the zeta potential of pyrite treated by $KMnO_4$ and SEX was 4 mV lower than that only treated by $KMnO_4$ at pH 7. However, for the natural pyrite, the zeta potential was reduced by 11 mV after the SEX conditioning at pH 7. These results indicate that SEX could not adsorb onto the $KMnO_4$-treated pyrite surface efficiently, which may be caused by the presence of oxidized products on the $KMnO_4$-treated pyrite surface preventing the adsorption of the collector.

In terms of chalcopyrite, the pH_{iep} of natural chalcopyrite was less than pH 4 (Fig. 6b), which agrees well with the previous findings (Hong et al., 2017; Khoso et al., 2019; Mu et al., 2016). Similar to pyrite, the zeta potential of chalcopyrite obviously decreased by 10 mV after the treatment with SEX at pH 7, suggesting that the SEX anions were strongly absorbed onto the chalcopyrite surfaces. In contrast, the conditioning with $KMnO_4$ barely changed the zeta potential of chalcopyrite. It was inferred that $KMnO_4$ could not oxidize the chalcopyrite surface efficiently to produce new surface species. Similarly, other oxidants, involving potassium ferrate, sulfuric acid and Carboxymethyl cellulose (Xie et al., 2021; Zheng et al., 2023), cannot react efficiently with chalcopyrite. It seems that pyrite rather than chalcopyrite is more readily to reacted with an oxidant.

On the other hand, for the $KMnO_4$-treated chalcopyrite, the further conditioning with SEX lowered the zeta potential by 4 mV at pH 7. This result implies that the SEX collector could still adsorb on the $KMnO_4$-

treated chalcopyrite surface. Therefore, the $KMnO_4$-treated chalcopyrite still can be floated by the SEX collector. The same conclusion was also obtained from above flotation and contact angle results.

XPS analysis of pyrite surface

Our zeta potential analysis reveals that $KMnO_4$ may oxidize the pyrite surface rather than the chalcopyrite surface. Aimed at identifying the surface oxidized species, the chemical states of elements on pyrite and chalcopyrite surfaces were evaluated by the XPS technique, since this technique can distinguish the oxidized state of an element based on the binding energy (BE) of core-level electrons of the element.

Figure 7 displays the narrow-scan Fe 2p spectra of the natural and $KMnO_4$-treated pyrite samples. Only one Fe component at 707. 45 eV was observed on the natural pyrite surface, and attributed to the Fe in the pyrite lattice (Khoso et al., 2019). Differently, in addition to the Fe in the pyrite lattice (BE of 707.52 eV), another Fe component located at a higher BE level (711.42 eV) was also observed in the XPS spectrum of the $KMnO_4$-treated pyrite sample. Generally, the higher BE of an element, the higher the oxidation state of the element. Such Fe specie at 711.42 eV could be assigned to FeO/FeOOH species (Chimonyo et al., 2017). It seems that the treatment of $KMnO_4$ oxidized the pyrite surface, producing surface oxidized species. In addition, 83% of Fe atoms on the oxidized surface was in the form of FeO/FeOOH, implying that the FeO/FeOOH species was the dominant species on the $KMnO_4$-treated pyrite surface.

The S components on the natural and $KMnO_4$-treated pyrite surfaces were also determined by the XPS method (Fig. 8). In the XPS spectrum of the natural pyrite, the BEs of S $2p_{3/2}$ and S $2p_{1/2}$ were 162.89 eV and 164.07 eV, respectively (Fig. 8). These BE results are consistent with a previous report about pyrite (Khoso et al., 2019). Two finite XPS peaks at 169.94 eV and 168.76 eV were also detected in the spectrum and could be attributed to SO_4^{2-} in $Fe_2(SO_4)_3$ (Khoso et al., 2019). Due to the high solubility of $Fe_2(SO_4)_3$, it is rational to predict that $Fe_2(SO_4)_3$ may be not present on the pyrites surface (Jin et al., 2015) and such XPS speaks were from SO_4^{2-} species. It appears that the natural pyrite surface was slightly oxidized by the oxygen in the air. For the $KMnO_4$-treated pyrite, the BEs of the S $2p_{3/2}$ and S $2p_{1/2}$ peaks of pyrite were 162.84 eV and 164.02 eV, similar to the results from natural pyrite. However, the XPS peaks of SO_4^{2-} at 168.73 eV and 169. 91 eV were stronger than those of the natural pyrite. The atomic ratio of the S in SO_4^{2-} to the S in pyrite reached 0.52:1. These results imply that the S atom on the pyrite surface can also be oxidized by the $KMnO_4$ in the solution.

The above XPS results clarify that $KMnO_4$ conditioning can oxidize Fe and S atoms on the pyrite surface, generating FeO/FeOOH and SO_4^{2-}. These oxides may reduce the hydrophobicity of pyrite and inhibit the adsorption of the SEX collector on the pyrite surface, accounting for the poor recovery of $KMnO_4$-treated pyrite.

XPS analysis of chalcopyrite surface

The chemical environments of atoms on chalcopyrite surfaces were also examined for comparison. The Cu XPS spectra of the natural and $KMnO_4$-treated chalcopyrite are plotted in Fig. 9. The BE of Cu $2p_{3/2}$ from chalcopyrite was 932.51 eV (Xie et al., 2021). Another Cu $2p_{3/2}$ peak was found at a higher BE position, i.e., 933.64 eV, due to the CuO present on the chalcopyrite surface (Khoso et al., 2019). Such oxide species may araise from the oxidation during the sample preparation. It was noted that the peak area of CuO was much smaller than that of Cu in chalcopyrite, indicating that the oxidation of the natural chalcopyrite surface was limited.

For the $KMnO_4$-treated chalcopyrite, the $KMnO_4$ treatment could not alter the Cu BE of chalcopyrite or CuO. However, the dominant Cu species was still the Cu from chalcopyrite. It appears that the $KMnO_4$ treatment could not efficiently oxidize the chalcopyrite surface or alter the chemical state of Cu atoms in chalcopyrite.

In terms of the S spectra, the major S peaks of the natural chalcopyrite were in the BE region of 160–166 eV (Fig. 10). The S $2p_{3/2}$ peaks at 161.19 eV and 163.68 eV corresponded to S and S_n^{2-} on the chalcopyrite surface (Chimonyo et al., 2017). An oxidized S specie with a BE of 168.75 eV was detected in the XPS spectrum, and was from the $Fe_2(SO_4)_3$ component. As the chalcopyrite was treated with $KMnO_4$, the BEs of S_n^{2-} and S were almost the same as those of natural chalcopyrite. It appears that the $KMnO_4$ treatment did not result in efficient oxidation of the chalcopyrite surface. Therefore, oxidized products were limited on the chalcopyrite surface. For this reason, the chalcopyrite surface maintained a satisfactory hydrophobicity after the $KMnO_4$ condition and could be floated efficiently by the SEX collector.

SEM-EDS studies

SEM-EDS is a powerful technique for characterizing the morphology study and the elemental distribution of mineral surface (Chen et al., 2020). SEM exhibits allows for the observation of highly magnified, and thus, a few nanometers of a mineral surface can be detected to obtain a fine-resolution image (Chen et al., 2023). Because of this advantage of SEM, the features of the elemental distribution on pyrite and chalcopyrite surfaces were detected by the SEM-EDS system, aiming to reveal the difference in the oxidation levels of the two mineral surfaces.

Figure 11 compares the distributions of O, Fe, and S atoms on the natural and the $KMnO_4$-treated pyrite surfaces. The O, Fe, and S atoms were found throughout the whole examined area on the natural pyrite surface (Fig. 11a). However, the O concentration was only 4.61%, which was much lower than that of the Fe or S atoms (Fig. 12). This result showed that the natural pyrite has been slightly oxidized, which agrees well with our XPS results. In terms of the $KMnO_4$-treated pyrite, O, Fe and S atoms distributed on the examined pyrite surface (Fig. 11b). However, the O concentration increased by 10% compared to that on the natural pyrite surface. This increase in O concentration may be caused by the FeO/FeOOH and SO_4^{2-} species on the oxidized pyrite surface. The S concentration on the oxidized pyrite surface was 20%

lower than that on the natural surface. It is expected that the formed SO_4^{2-} species on the pyrite surface may be released from the surface and dissolved into the solution, due to the high solubility of $Fe_2(SO_4)_3$.

In addition, Miller et al. reported that oxidized islands are formed on the oxidized pyrite surface (Jin et al., 2015). Differently, the O atoms arising from oxidized species were uniformly distributed on the pyrite surface in this work. Such discrepancy may be caused by the difference in the sample preparation for SEM analysis. A pyrite plane was used in the work of Miller et al. However, fine pyrite particles were used in this study, and the pyrite slurry was intensely stirred to achieve complete oxidation. Thus, pyrite particle surface featured a diverse distribution of oxidized components.

In the case of natural chalcopyrite, Cu, Fe, and S atoms were detected and well-distributed on the mineral surface (Fig. 13a). It is found that O atoms (4.59% of concentration) existed on the chalcopyrite surface and coated the surface evenly (Figs. 13a and 14). Such O-containing products were also found by our XPS analysis and may result from the oxidation during the sample preparation process. On the other hand, the above elements were also observed on the entire $KMnO_4$-treated chalcopyrite surface (Fig. 13b). However, the $KMnO_4$-treatment was unable to notably alter the elemental concentrations on the chalcopyrite surface. As a result, the variation in elemental concentrations was less than 2% (Fig. 14). Our XPS results also illustrated that $KMnO_4$ could not efficiently oxidize the chalcopyrite surface. Therefore, the atomic concentrations on the $KMnO_4$-treated surface were approximate to those on the natural surface.

In summary, although SEM-EDS cannot identify the oxidation products on the pyrite or chalcopyrite surface, this technique reveals the distribution features of such products. The FeO/FeOOH species were well coated on the $KMnO_4$-treated pyrite surface, which contributes to the hydrophilicity of pyrite. On the contrary, no extra oxidation products were generated on the $KMnO_4$-treated chalcopyrite surface, explaining the good floatability of $KMnO_4$-treated chalcopyrite.

Conclusions

$KMnO_4$ is a specific depressant for pyrite in the pyrite-chalcopyrite system. This depressant should be used at pH 7 and its concentration should be less than 4×10^{-4} mol/L, to obtain a satisfactory separation efficiency.

$KMnO_4$ could react with the pyrite surface, lowering the hydrophobicity of pyrite and increasing its zeta potential. The oxidation components on the $KMnO_4$-treated surface were FeO, FeOOH and SO_4^{2-} species. These components uniformly coated the pyrite surface, resulting in a poor recovery of pyrite. In contrast, the chemical states of elements on chalcopyrite surface could not be verified by the $KMnO_4$ conditioning, and thus chalcopyrite could still be floated by the xanthate collector. Thus, the separation of pyrite from chalcopyrite is achieved with $KMnO_4$ as a depressant.

Declarations

Conflicts of Interest:

The authors declare no conflict of interest.

Acknowledgements

Financial support from National Natural Science Foundation of China (22068020), and the Yong Top-notch Talent Project of Yunnan Ten Thousand Talent Plan (Yunnan Province, PR China) is gratefully acknowledged.

References

1. Bahrami A, Ghorbani Y, Hosseini MR, Kazemi F, Abdollahi M, Danesh A (2018) Combined Effect of Operating Parameters on Separation Efficiency and Kinetics of Copper Flotation. Min Metall Explor 36:409–421. https://doi.org/10.1007/s42461-018-0005-y
2. Bai X, Liu J, Feng QC, Wen SM, Dong WC, Lin YL (2021) Study on selective adsorption of organic depressant on chalcopyrite and pyrite surfaces. Colloids Surf A 627:127210. https://doi.org/10.1016/j.colsurfa.2021.127210
3. Chen X, Gu GH, Li LJ, Zhu RF (2018) The selective effect of food-grade guar gum on chalcopyrite-monoclinic pyrrhotite separation using mixed aerofloat (CSU11) as collector. Int J Miner Metall Mater 25:1123–1131. https://doi.org/10.1007/s12613-018-1663-y
4. Chen YY, Chen Y, Liu Q, Liu X (2023) Quantifying common major and minor elements in minerals/rocks by economical desktop scanning electron microscopy/silicon drift detector energy-dispersive spectrometer (SEM/SDD-EDS). Solid Earth Sci 8(1):49–67. https://doi.org/10.1016/j.sesci.2022.12.002
5. Chen YG, Feng B, Guo YT, Wang T, Zhang LZ, Zhong CH, Wang HH (2021) The role of oxidizer in the flotation separation of chalcopyrite and galena using sodium lignosulfonate as a depressant. Min Eng 172:107160. https://doi.org/10.1016/j.mineng.2021.107160
6. Chen YG, Feng B, Peng JX, Wang ZM (2022) Selective flotation of galena from sphalerite using a combination of KMnO4 and carboxylated chitosan. Appl Surf Sci 602:154412. https://doi.org/10.1016/j.apsusc.2022.154412
7. Chen ZH, Liu XJ, Yang JJ, Little E, Zhou Y (2020) Deep learning-based method for SEM image segmentation in mineral characterization, an example from Duvernay Shale samples in Western Canada Sedimentary Basin. Comput Geosci 138:104450. https://doi.org/10.1016/j.cageo.2020.104450

8. Chimonyo W, Wiese J, Corin K, O'Connor C (2017) The use of oxidising agents for control of electrochemical potential in flotation. Min Eng 109:135–143. https://doi.org/10.1016/j.mineng.2017.03.011
9. Deng W, Xu LH, Tian J, Hu YH, Han YX (2017) Flotation and Adsorption of a New Polysaccharide Depressant on Pyrite and Talc in the Presence of a Pre-Adsorbed Xanthate Collector. Miner 7(3):40. https://doi.org/10.3390/min7030040
10. Ding Z, Bi YX, Li J, Yuan JQ, Dai HX, Bai SJ (2022) Flotation separation of chalcopyrite and pyrite via Fenton oxidation modification in a low alkaline acid mine drainage (AMD) system. Min Eng 187:107818. https://doi.org/10.1016/j.mineng.2022.107818
11. Dong JS, Liu QJ, Subhonqulov SH (2021) Effect of dextrin on flotation separation and surface properties of chalcopyrite and arsenopyrite. Water Sci Technol 83:152–161. https://doi.org/10.1016/j.colsurfa.2020.124669
12. Han G, Wen SM, Wang H, Feng QC (2019) Effect of starch on surface properties of pyrite and chalcopyrite and its response to flotation separation at low alkalinity. Min Eng 143:106015. https://doi.org/10.1016/j.mineng.2019.106015
13. Han G, Wen SM, Wang H, Feng QC (2020) Selective adsorption mechanism of salicylic acid on pyrite surfaces and its application in flotation separation of chalcopyrite from pyrite. Sep Purif Technol 240:116650. https://doi.org/10.1016/j.seppur.2020.116650
14. Hong G, Choi J, Han Y, Yoo KS, Kim K, Kim SB, Kim H (2017) Relationship between Surface Characteristics and Floatability in Representative Sulfide Minerals: Role of Surface Oxidation. Mater Trans 58:1069–1075. https://doi.org/10.2320/matertrans.M2017014
15. Jiang K, Han YX, Liu J, Wang Y, Ge WC, Zhang DJ (2023) Experimental and theoretical study of the effect of pH level on the surface properties and floatability of pyrite. Appl Surf Sci 615:156350. https://doi.org/10.1016/j.apsusc.2023.156350
16. Jin JQ, Miller JD, Dang LX, Wick CD (2015) Effect of surface oxidation on interfacial water structure at a pyrite (100) surface as studied by molecular dynamics simulation. Int J Miner Process 139:64–76. https://doi.org/10.1016/j.minpro.2015.04.006
17. Khoso SA, Hu YH, Lu F, Gao Y, Liu RQ, Sun W (2019) Xanthate interaction and flotation separation of H_2O_2-treated chalcopyrite and pyrite. Trans Nonferrous Met Soc China 29:2604–2614. https://doi.org/10.1016/S1003-6326(19)65167-8
18. Li YB, Li WQ, Wei ZL, Xiao Q, Lartey C, Li YJ, Song SX (2019) The Influence of Common Chlorides on the Adsorption of SBX on Chalcopyrite Surface during Flotation Process. Min Process Extr Metall Rev 40:129–140. https://doi.org/10.1080/08827508.2018.1497625
19. Liu DZ, Zhang GF, Chen YF, Huang GH, Gao YW (2020) Investigations on the utilization of konjac glucomannan in the flotation separation of chalcopyrite from pyrite. Min Eng 145:106098. https://doi.org/10.1016/j.mineng.2019.106098
20. Liu RZ, Li JL, Wang YW, Liu DW (2020) Flotation separation of pyrite from arsenopyrite using sodium carbonate and sodium humate as depressants. Colloids Surf A 595:124669.

https://doi.org/10.1016/j.colsurfa.2020.124669

21. Liu Y, Liu Q (2004) Flotation separation of carbonate from sulfide minerals, I: flotation of single minerals and mineral mixtures. Min Eng 17:855–863. https://doi.org/10.1016/j.mineng.2004.03.006
22. Ma YQ, Yang MY, Tang LF, Zheng SL, Fu YF, Sheng QY, Yin WZ (2022) Flotation separation mechanism for secondary copper sulfide minerals and pyrite using novel collector ethyl isobutyl xanthogenic acetate. Colloids Surf A 634:128010. https://doi.org/10.1016/j.colsurfa.2021.128010
23. Moimane T, Huai YY, Peng YJ (2021) Evaluating the sulphidisation and flotation of oxidised chalcopyrite. Min Eng 164:106816. https://doi.org/10.1016/j.mineng.2021.106816
24. Mu YF, Peng YJ, Lauten RA (2016) The depression of copper-activated pyrite in flotation by biopolymers with different compositions. Min Eng 96–97:113–122. https://doi.org/10.1016/j.mineng.2016.06.011
25. Mu YF, Peng YJ, Lauten RA (2018) The galvanic interaction between chalcopyrite and pyrite in the presence of I lignosulfonate-based biopolymers and its effects on flotation performance. Min Eng 122:91–98. https://doi.org/10.1016/j.mineng.2018.03.048
26. Niu XP, Chen JH, Li YQ, Xia LY, Li L, Sun HY, Ruan R (2019) Correlation of surface oxidation with xanthate adsorption and pyrite flotation. Appl Surf Sci 495:143411. https://doi.org/10.1016/j.apsusc.2019.07.153
27. Owusu C, Fornasiero D, Addai-Mensah J, Zanin M (2014) Effect of regrinding and pulp aeration on the flotation of chalcopyrite in chalcopyrite/pyrite mixtures. Powder Technol 267:61–67. https://doi.org/10.1016/j.powtec.2014.06.02
28. Pan ZC, Liu ZC, Xiong JJ, Li JL, Wei Q, Zhang ZQ, Jiao F, Qin WQ (2022) Application and depression mechanism of sodium sulfite on galena-pyrite mixed concentrate flotation separation: Huize Lead-Zinc Mine, China, as an example. Min Eng 185:107696. https://doi.org/10.1016/j.mineng.2022.107696
29. Wang CT, Liu RQ, Khoso SA, Lu HY, Sun W, Ni ZY, Lyu F (2020) Combined inhibitory effect of calcium hypochlorite and dextrin on flotation behavior of pyrite and galena sulphides. Min Eng 150:106274. https://doi.org/10.1016/j.mineng.2020.106274
30. Wang CT, Liu RQ, Zhai QL, Wu MR, Jing NW, Xie FF, Sun W (2022) Influence of calcium and ferric ions on the depression of chalcopyrite by CMC: Flotation performance and adsorption mechanism study. Min Eng 184:107667. https://doi.org/10.1016/j.mineng.2022.107667
31. Wang X, Liu J, Zhu YM, Han YX (2021) Adsorption and depression mechanism of an eco-friendly depressant PCA onto chalcopyrite and pyrite for the efficiency flotation separation. Colloids Surf A 620:126574. https://doi.org/10.1016/j.colsurfa.2021.126574
32. Wei Z, Wang H, Xue C, Zeng M (2019) Selective depression of sphalerite by combined depressant $K_3[Fe(CN)_6]$, $ZnSO_4$, and Na_2CO_3 in Pb–Zn sulfide flotation separation. Chem Pap 74(2):421–429. https://doi.org/10.1007/s11696-019-00884-w
33. Wu SH, Wang JJ, Tao LM, Fan RH, Wang C, Sun W, Gao ZY (2022) Selective separation of chalcopyrite from pyrite using an acetylacetone-based lime-free process. Min Eng 182:107584.

https://doi.org/10.1016/j.mineng.2022.107584

34. Xie HY, Liu YH, Rao B, Wu JZ, Gao LK, Chen LZ, Tian XS (2021) Selective passivation behavior of galena surface by sulfuric acid and a novel flotation separation method for copper-lead sulfide ore without collector and inhibitor. Sep Purif Technol 267:118621. https://doi.org/10.1016/j.seppur.2021.118621
35. Zhang HL, Zhang F, Sun W, Chen DX, Chen JH, Wang R, Han MJ, Zhang CY (2023) The effects of hydroxyl on selective separation of chalcopyrite from pyrite: A mechanism study. Appl Surf Sci 608:154963. https://doi.org/10.1016/j.apsusc.2022.154963
36. Zheng YX, Huang YS, Hu PJ, Qiu XH, Lv JF, Bao LY (2023) Flotation behaviors of chalcopyrite and galena using ferrate (VI) as a depressant. Int J Min Sci Technol 33:93–103. https://doi.org/10.1016/j.ijmst.2022.09.015

Figures

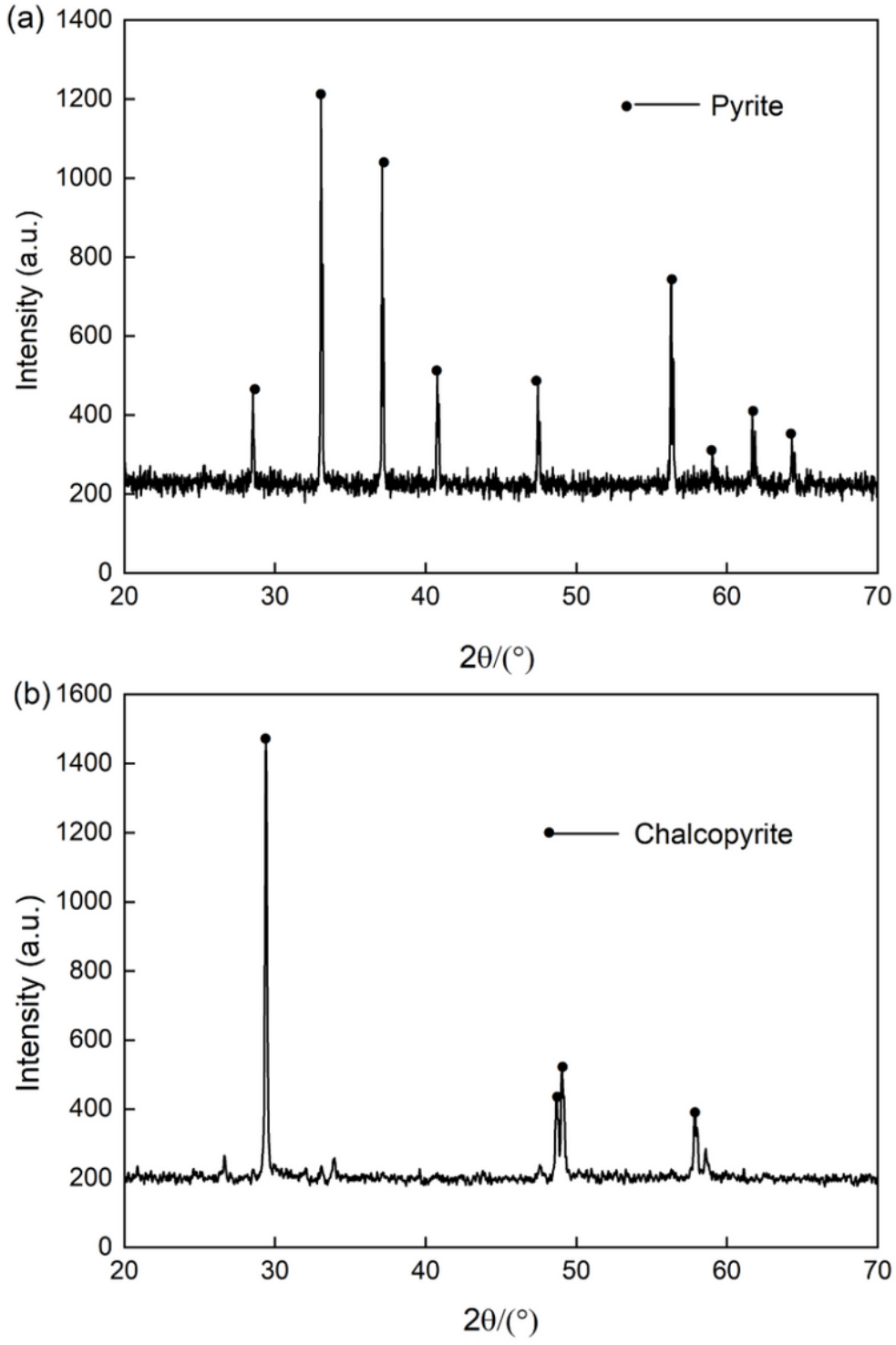

Figure 1

XRD patterns of pure mineral samples of pyrite (a) and chalcopyrite (b).

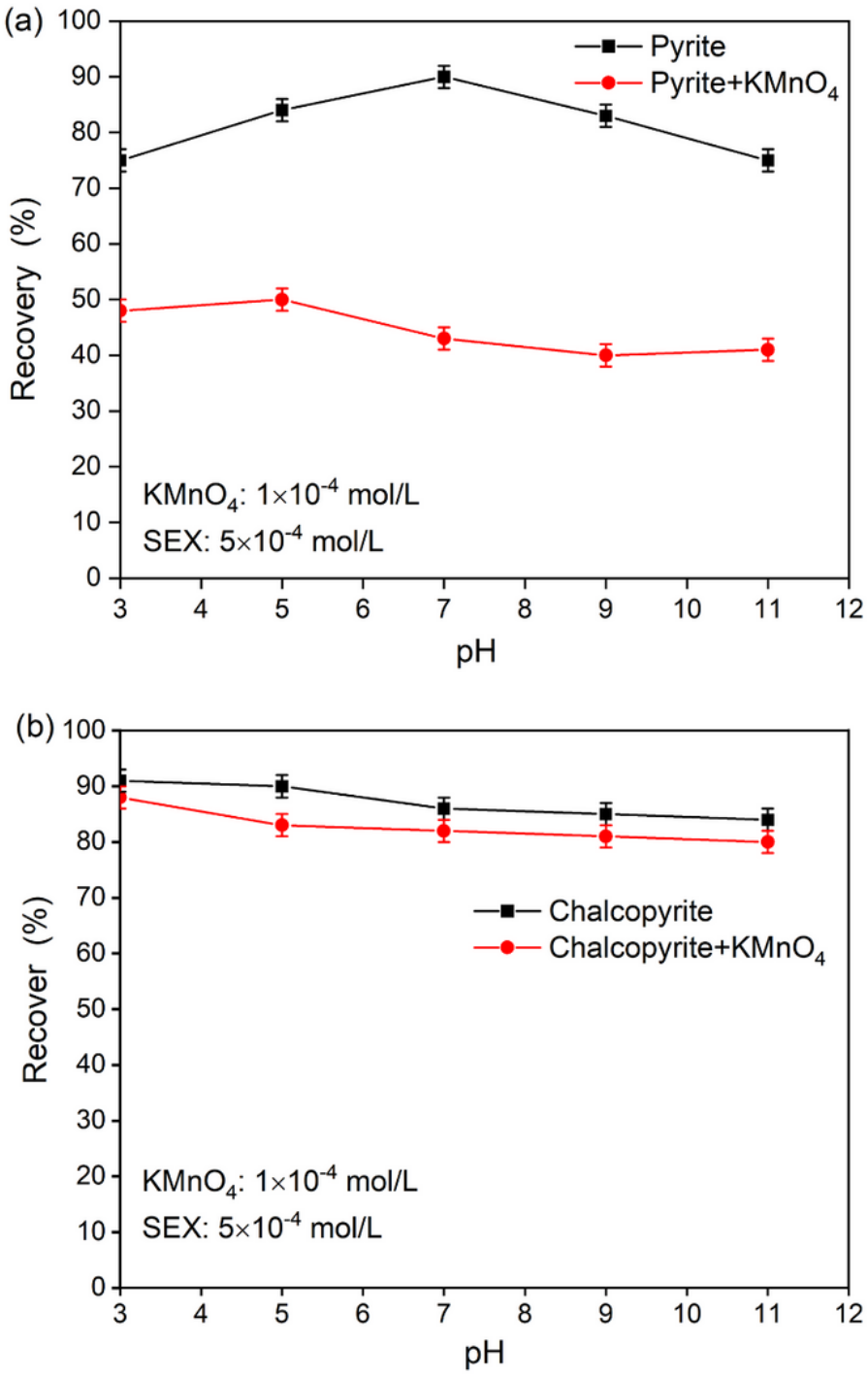

Figure 2

Flotation recoveries of pyrite (a) and chalcopyrite (b) before and after treatment with $KMnO_4$ (3 min of treatment) at different pH conditions.

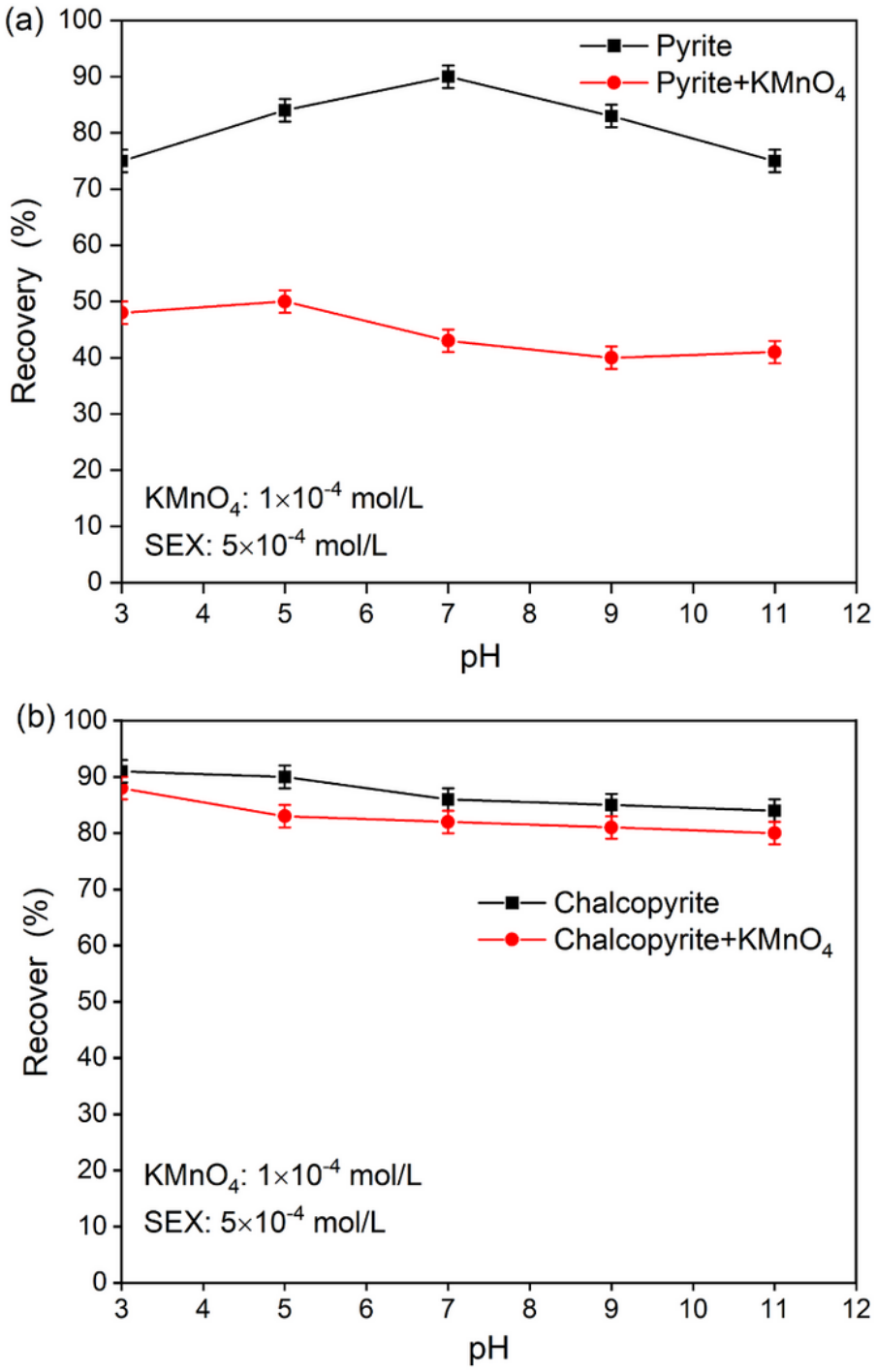

Figure 3

Flotation recoveries of pyrite (a) and chalcopyrite (b) with the $KMnO_4$ treatment depending on the treatment times.

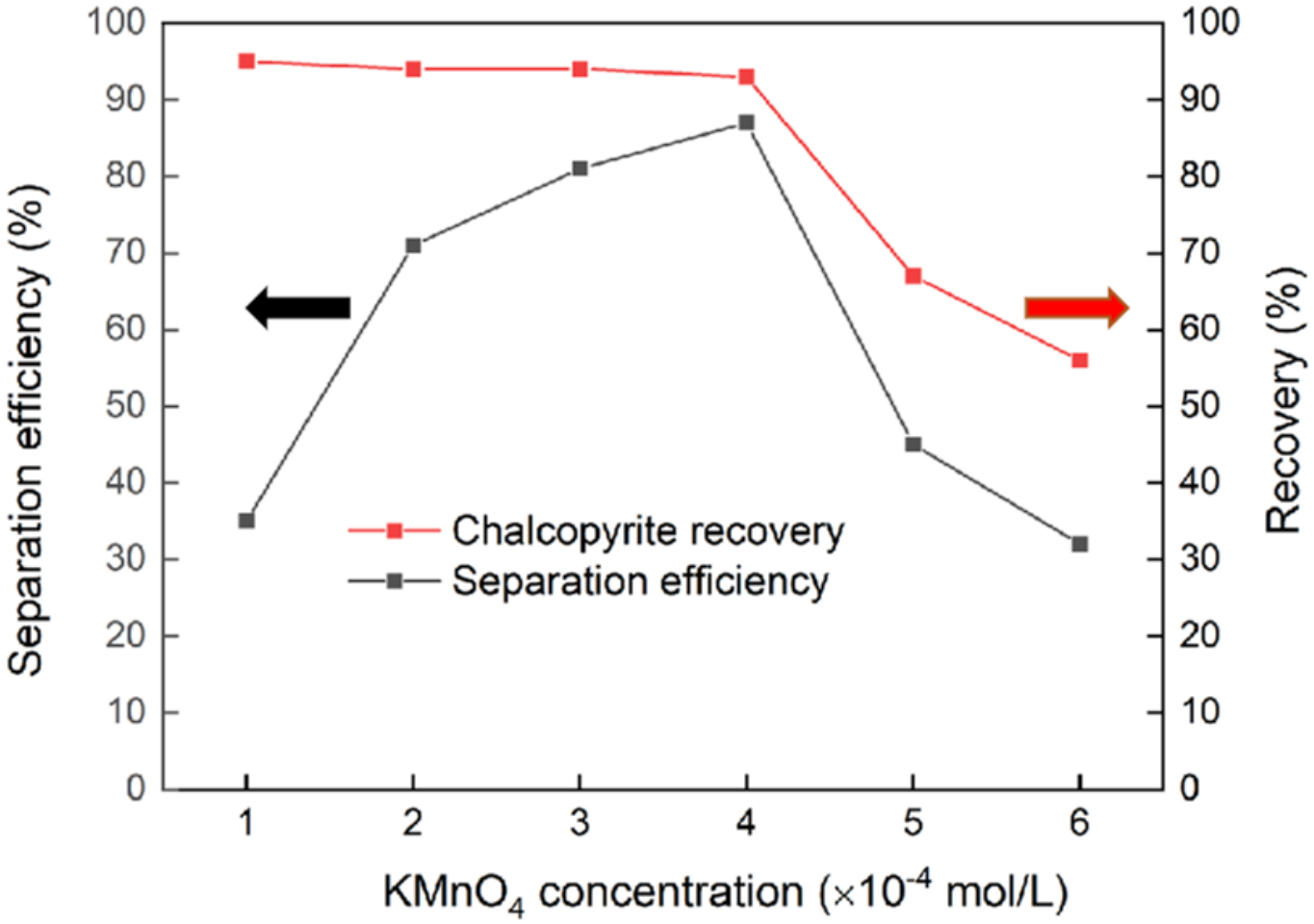

Figure 4

Flotation tests of pyrite and chalcopyrite mixture.

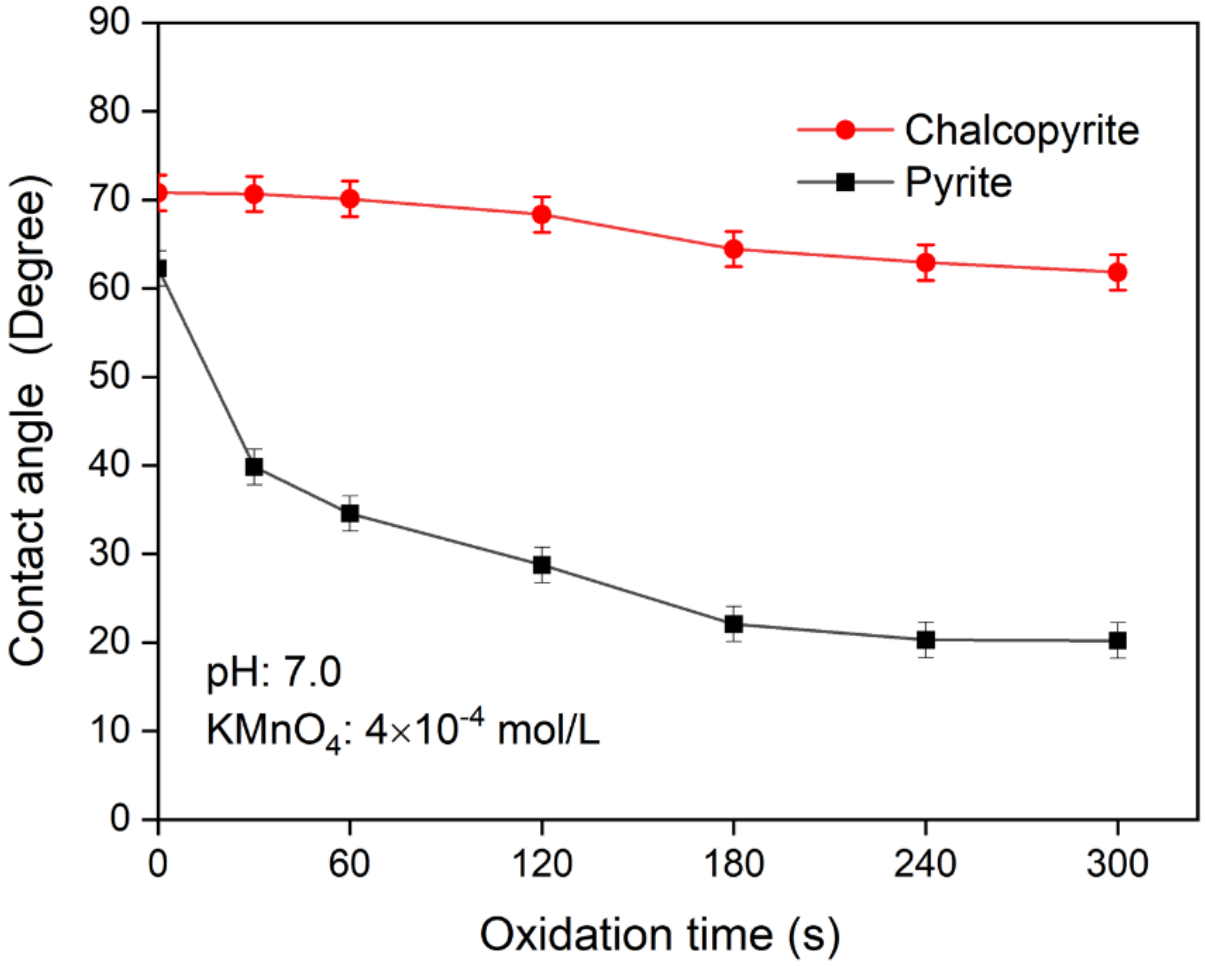

Figure 5

Contact angles of pyrite and chalcopyrite oxidized by KMnO4 for different times.

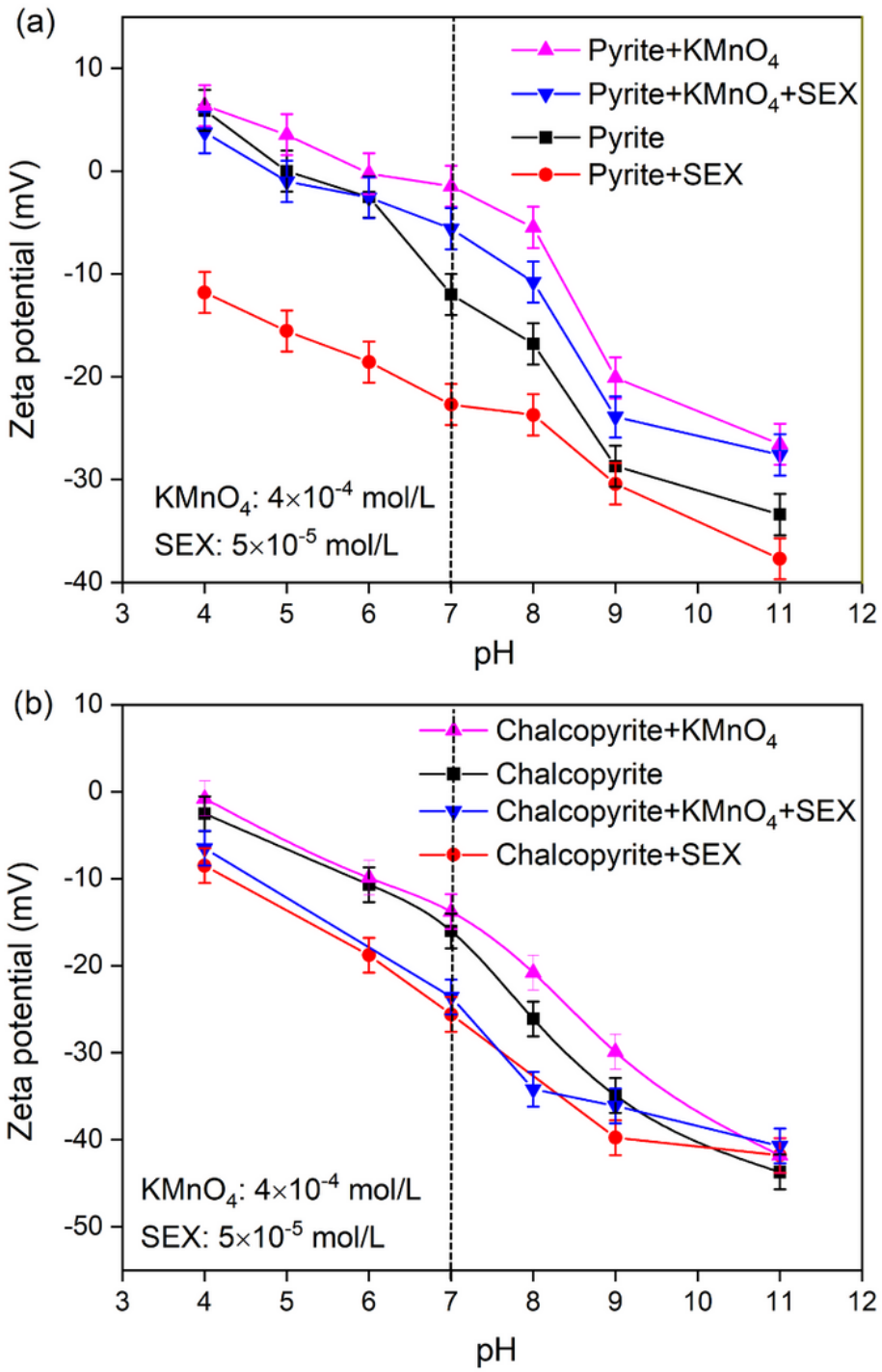

Figure 6

Zeta potential of pyrite (a) and chalcopyrite (b) before and after treatment with $KMnO_4$ and SEX.

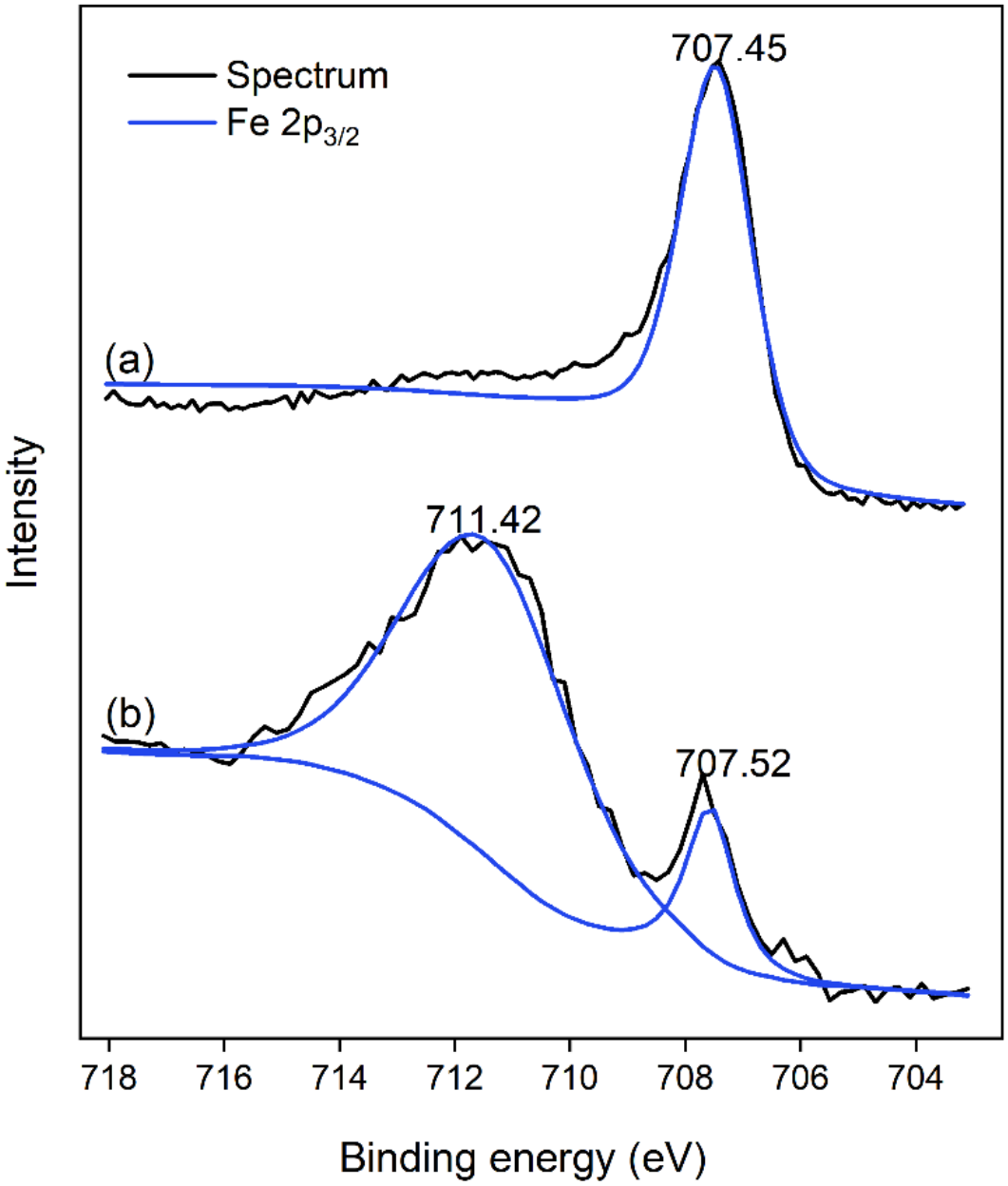

Figure 7

XPS spectra of Fe element of pyrite samples: (a) natural pyrite; (b) pyrite treated by $KMnO_4$ (4×10^{-4}mol/L).

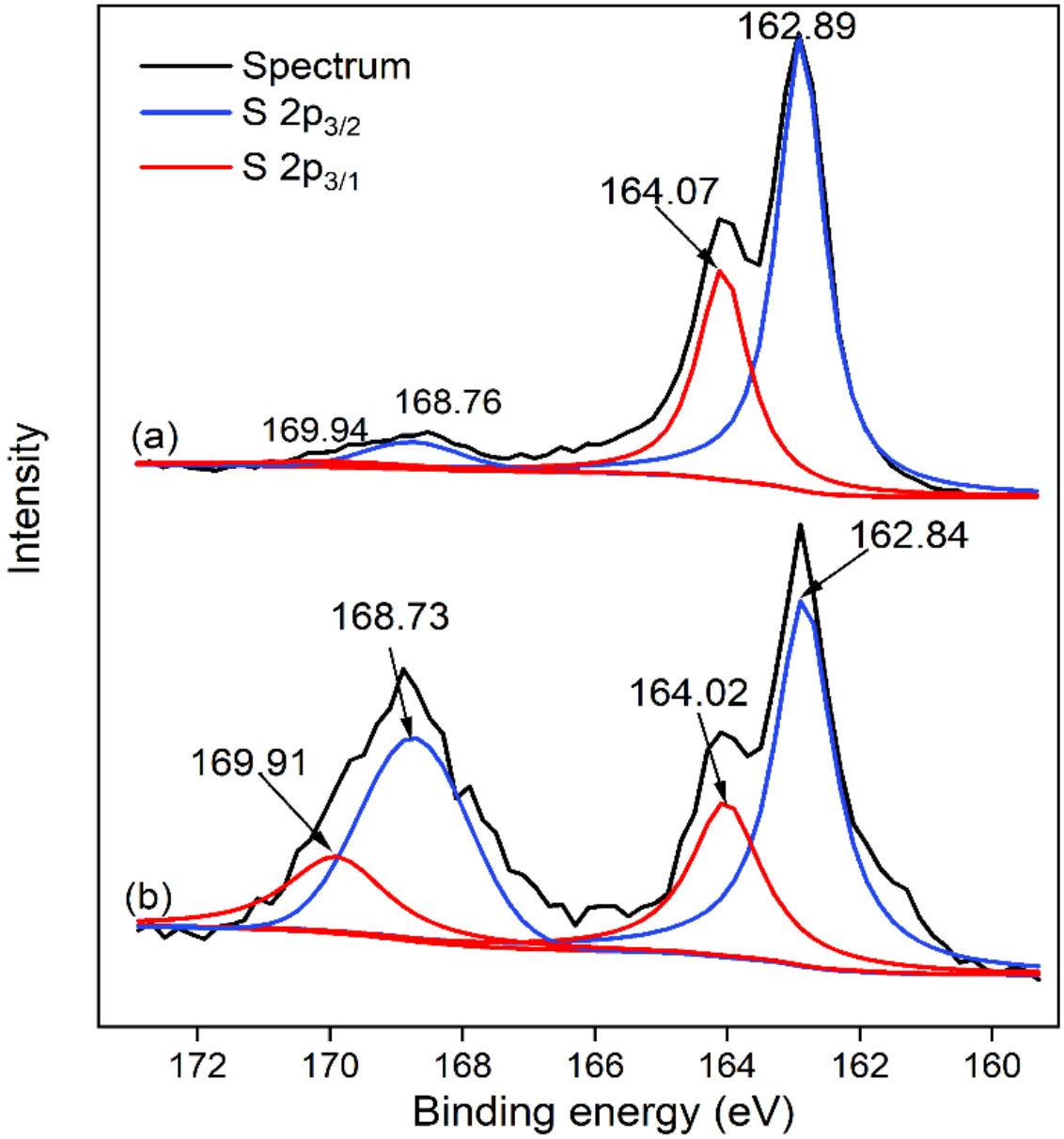

Figure 8

XPS spectra of S element of pyrite samples: (a) natural pyrite; (b) pyrite treated by $KMnO_4$ (4×10^{-4} mol/L).

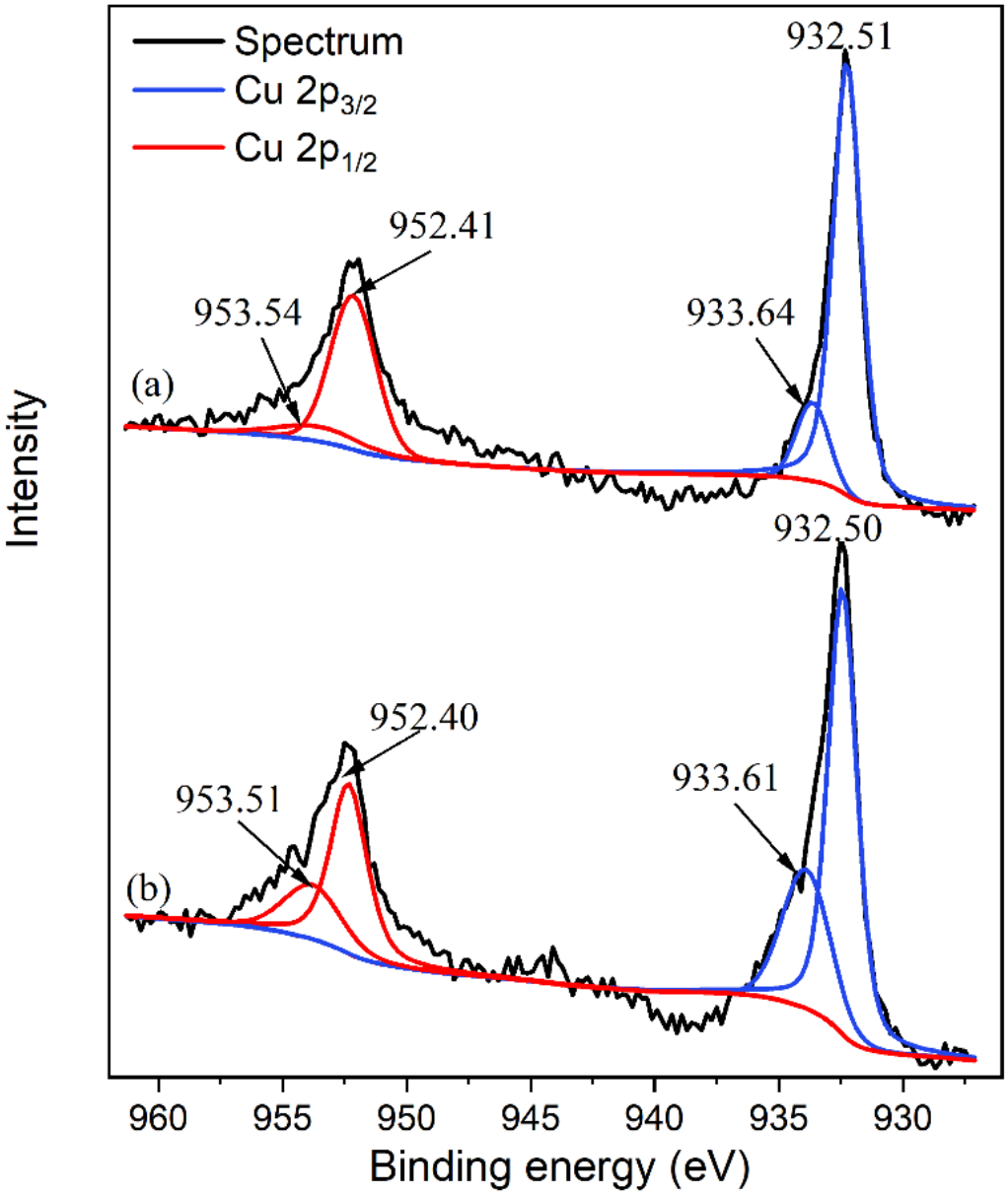

Figure 9

XPS spectra of Cu element of chalcopyrite samples: (a) natural chalcopyrite; (b) chalcopyrite treated by $KMnO_4$ (4×10^{-4} mol/L)

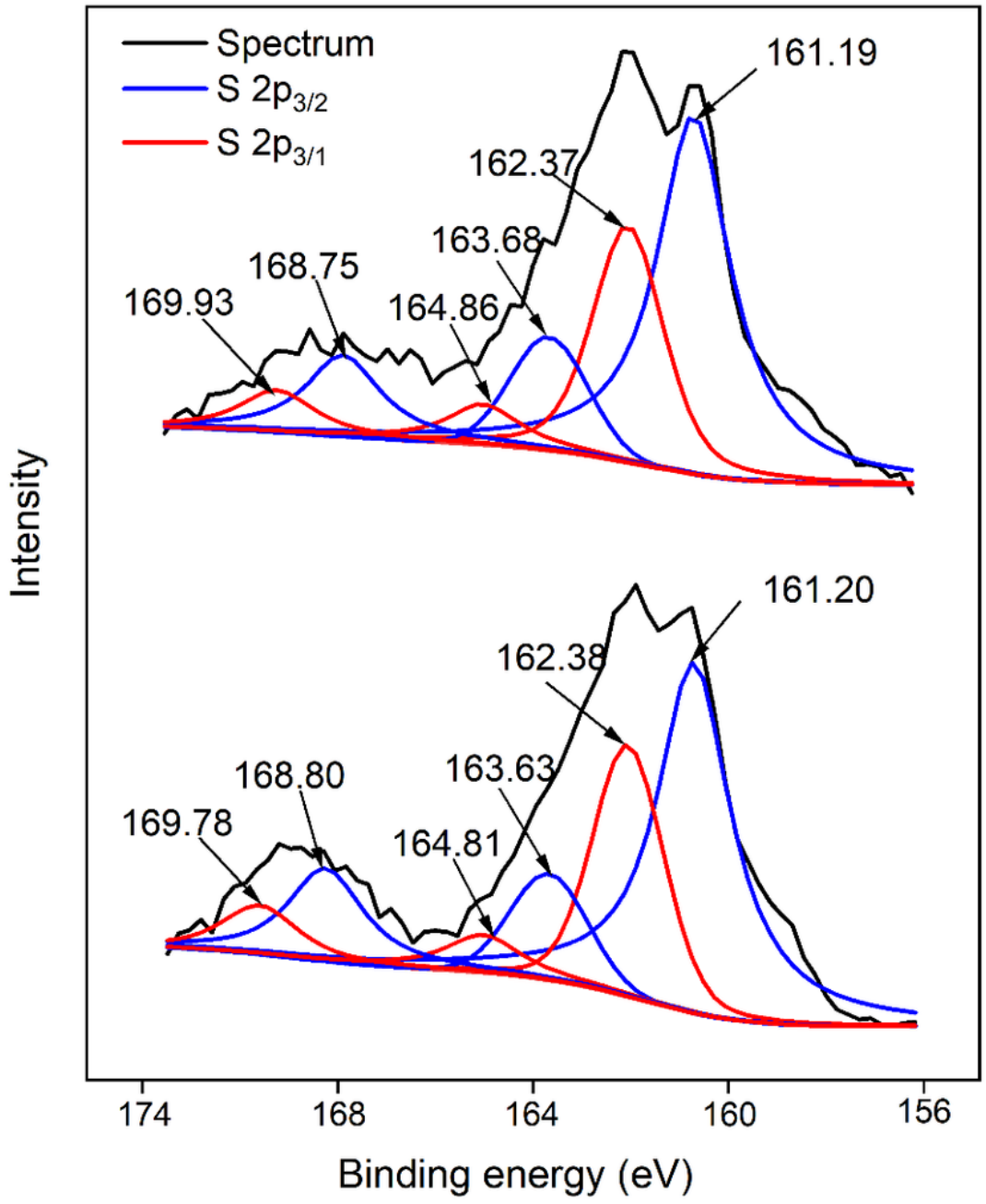

Figure 10

XPS spectra of S element of chalcopyrite samples: (a) natural chalcopyrite; (b) chalcopyrite treated by $KMnO_4$ (4×10^{-4} mol/L)

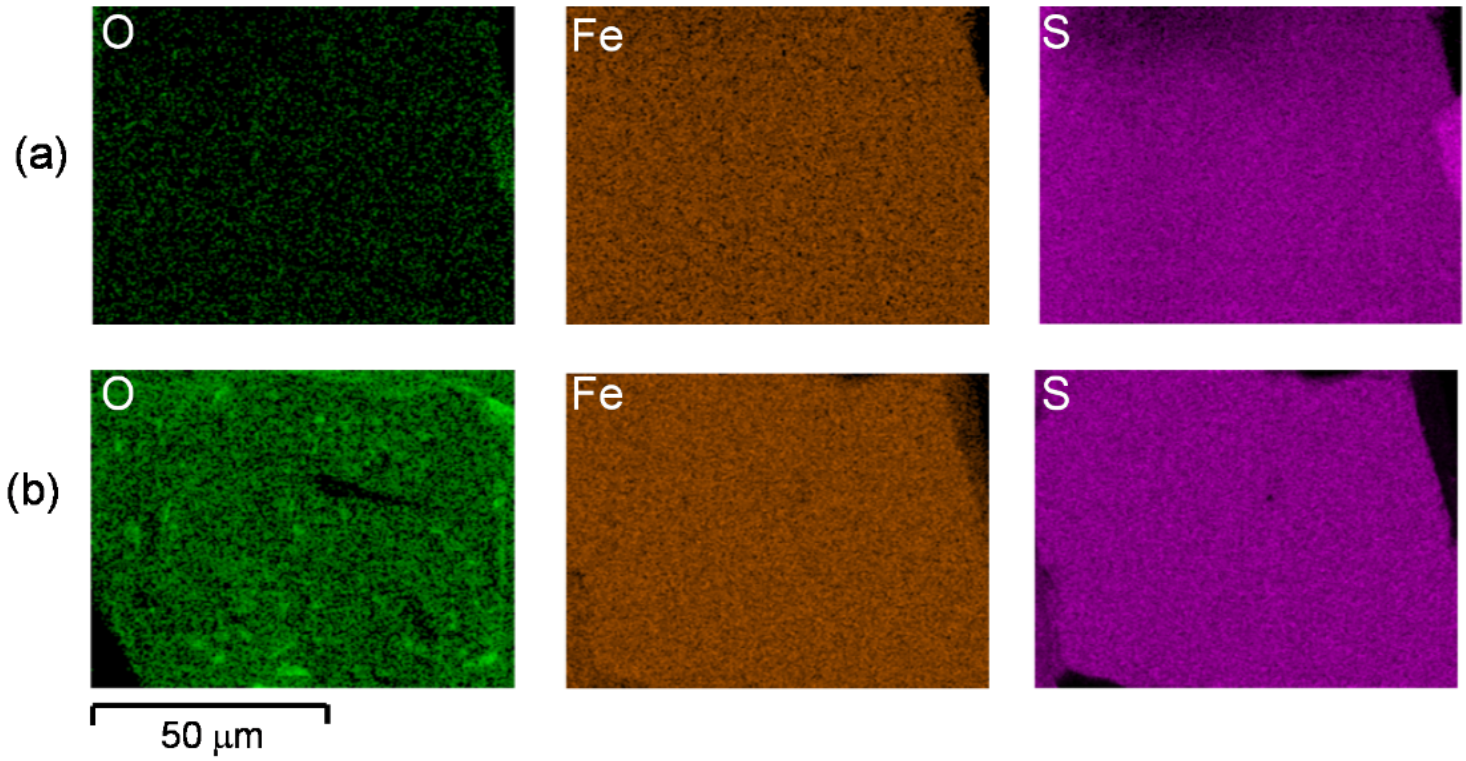

Figure 11

Scanning electron microscopy results of pyrite ((a) nature pyrite; (b) pyrite treated by $KMnO_4$ (4×10^{-4} mol/L).

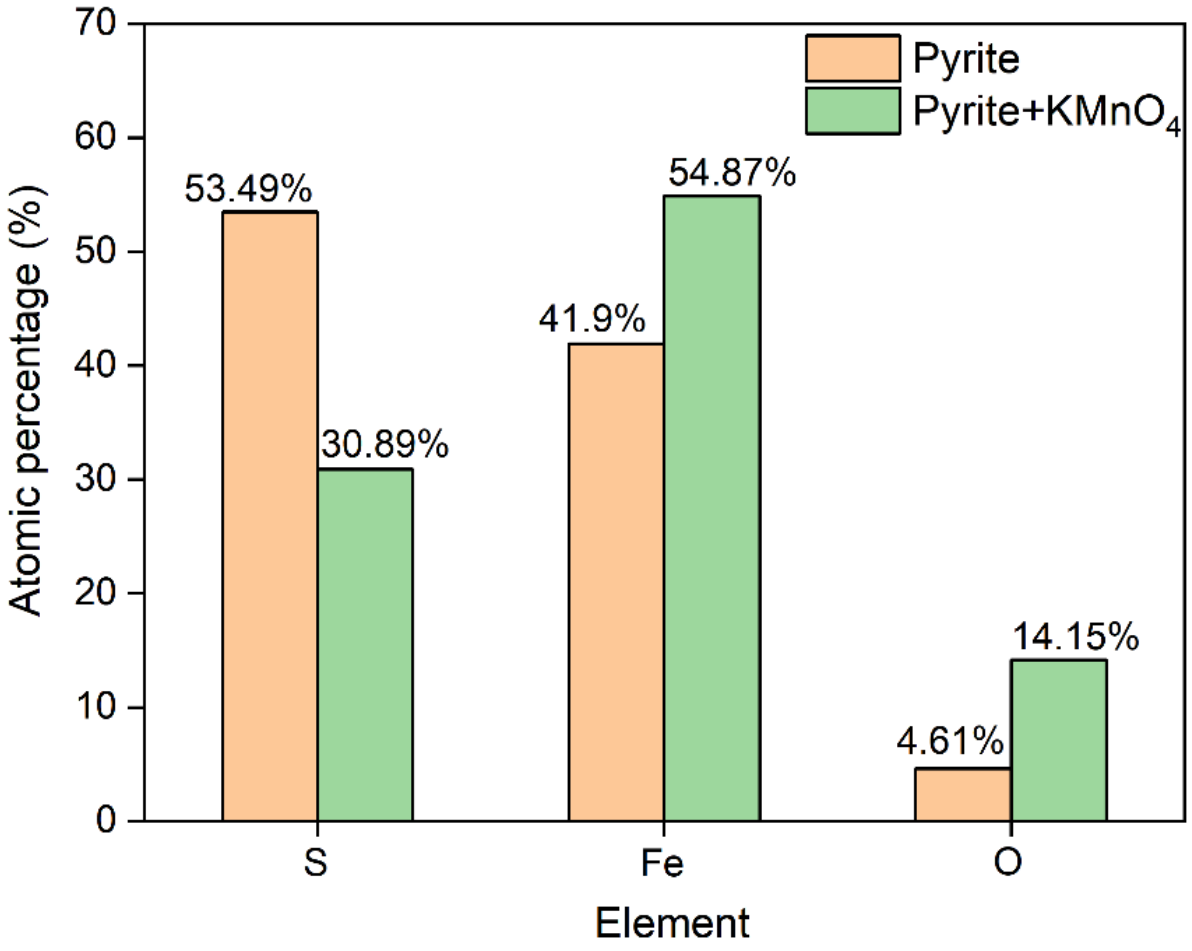

Figure 12

Distribution of pyrite surface elements with/without $KMnO_4$ (4×10^{-4} mol/L).

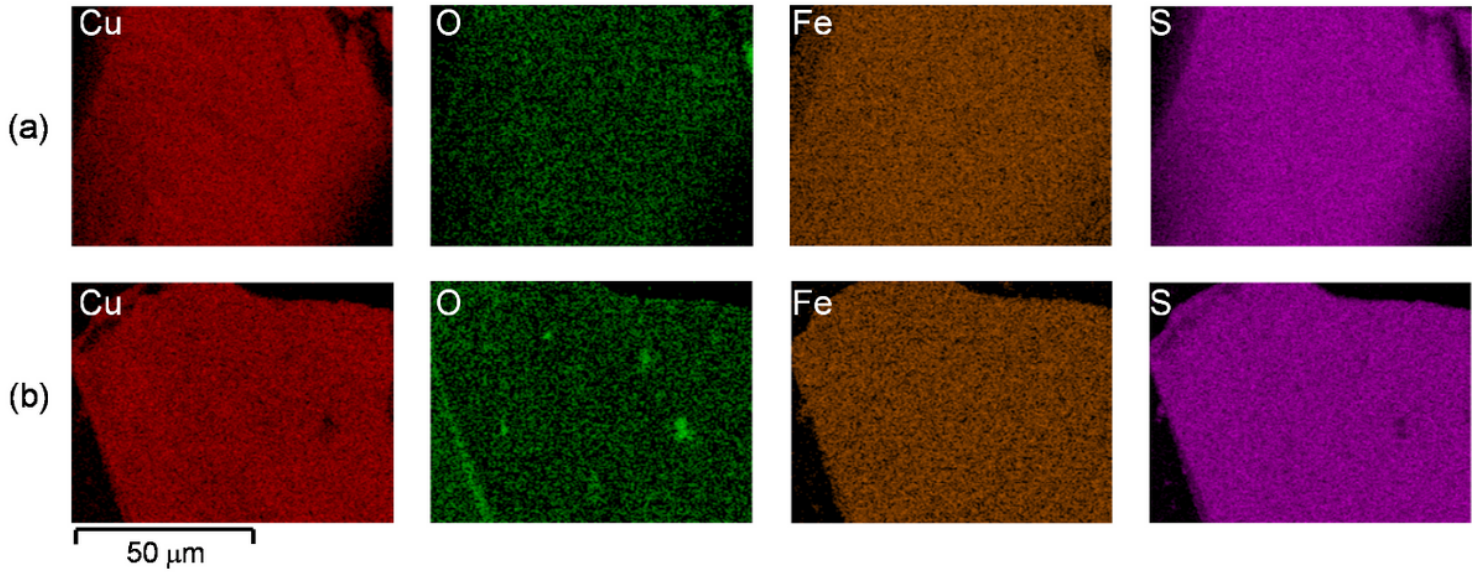

Figure 13

Scanning electron microscopy results of chalcopyrite ((a) nature chalcopyrite; (b) chalcopyrite treated by $KMnO_4$ (4×10^{-4} mol/L).

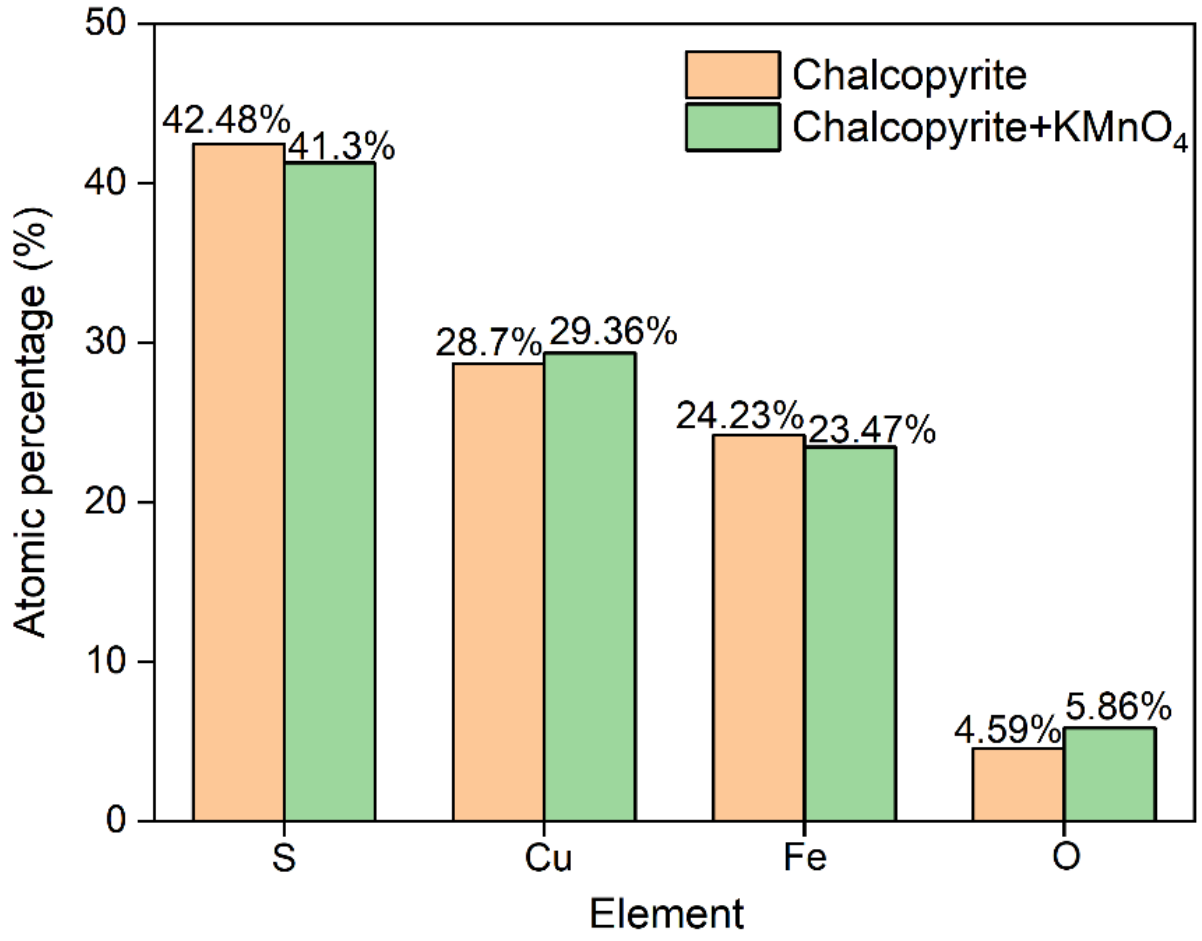

Figure 14

Distribution of chalcopyrite surface elements with/without $KMnO_4$ (4×10^{-4} mol/L).

Supplementary Files

This is a list of supplementary files associated with this preprint. Click to download.

- supplementarymaterial.docx